Official Journal of the Brain, Behaviour and Intellection Association

ACTA BIOSCIENTIA
Journal of Biomedical and Biological Sciences

Acta Bioscientia **2026**:2(2);458-472 OPEN ACCESS
https://doi.org/10.71181/actabioscientia12610

Histopathological and Computational Histomorphometric Evaluation of the Protective Effects of Quercetin in High-Fat High-Sugar Diet-Induced Metabolic Syndrome in Wistar Rats

ONAOLAPO Adejoke Y[1], AKINRINDE Eniola Sophia[2], WAHAB Karimot Abiola[2], OLOFINNADE Anthony T[3], ONAOLAPO Olakunle J[4*]

[1.]Behavioural Neuroscience/Neurobiology Unit, Department of Anatomy, Faculty of Basic Medical Sciences, Ladoke Akintola University of Technology, Ogbomoso, Oyo State, Nigeria. ayonaolapo@lautech.edu.ng ORCID: 0000-0001-7126-7050

[2.]Department of Medical Laboratory Science, Ladoke Akintola University of Technology, Ogbomoso, Oyo State, Nigeria

[3.]Department of Pharmacology, Therapeutics and Toxicology, Faculty of Basic Clinical Sciences, College of Medicine, Lagos State University, Ikeja, Lagos State. anthony.olofinnade@lasucom.edu.ng

[4.]Behavioural Neuroscience/Neuropharmacology Unit, Department of Pharmacology and Therapeutics, Faculty of Basic Clinical Sciences, Ladoke Akintola University of Technology, Ogbomoso, Oyo State, Nigeria. ojonaolapo@lautech.edu.ng ORCID: 0000-0003-2142-6046

*Corresponding Author

Abstract

Metabolic syndrome is increasingly associated with obesity, insulin resistance, type 2 diabetes mellitus, cardiovascular disease, and multi-organ dysfunction. This study investigated the protective effects of quercetin against high-fat/high-sugar (HFHS) diet-induced metabolic, hepatic, and renal alterations in Wistar rats. Adult rats (120–150 g) were randomly assigned into five groups (n = 6/group): control, HFHS, HFHS + quercetin 100 mg/kg (HFHS/Q100), HFHS + quercetin 200 mg/kg (HFHS/Q200), and HFHS + metformin 25 mg/kg (HFHS/MET). Metabolic, biochemical, histopathological, quantitative histomorphometric, colour histogram, and computational tissue analyses were performed. HFHS feeding significantly increased body weight, feed intake, blood glucose, plasma insulin, leptin, total cholesterol, triglycerides, LDL, malondialdehyde, TNF-α, liver enzymes, urea, and creatinine, while reducing adiponectin, total antioxidant capacity, and IL-10 levels. Histopathological examination revealed marked hepatic and renal structural alterations including hepatocellular vacuolation, sinusoidal distortion, tubular degeneration, glomerular disruption, and reduced tissue compactness. Quantitative histomorphometric and computational analyses demonstrated treatment-dependent alterations in cellular profile density, stained area fraction, optical density, texture entropy, and RGB staining characteristics. Quercetin supplementation significantly ameliorated HFHS-induced metabolic, oxidative, inflammatory, hepatic, and renal abnormalities. Quercetin improved glucose regulation, lipid profile, antioxidant status, adipokine balance, and organ integrity while partially restoring hepatic and renal histoarchitecture. Overall, quercetin demonstrated significant hepatoprotective and renoprotective effects against HFHS-induced metabolic syndrome, likely mediated through antioxidant, anti-inflammatory, and metabolic regulatory mechanisms.

KEYWORDS: Computational Histomorphometry, Diet, Inflammation, Lipid dysmetabolism, Metabolism, Nutrients

1. Introduction

Metabolic syndrome refers to a cluster of interrelated clinical conditions, including central obesity, hypertension, hyperglycaemia, hyperinsulinaemia, and dyslipidaemia [1-5]. The presence of any of these abnormalities is associated with a significantly increased risk of diabetes mellitus, cardiovascular disease, and cerebrovascular disease [5-8]. Importantly, these components often interact synergistically, further amplifying the risk of end-organ damage, morbidity, and mortality [6-9]. The global rise in the prevalence of metabolic syndrome has paralleled the increasing burden of type 2 diabetes mellitus and cardiovascular disease [10-12] Consequently, metabolic syndrome is now widely recognized as a major public health concern [5].

© The Author(s) 2026. Open Access This article is licensed under a Creative Commons Attribution-Non-Commercial-No Derivatives 4.0 International License, which permits any non-commercial use including sharing, distribution and reproduction in any medium or format, provided appropriate credit is given to the original author(s) and the source, providing a link to the Creative Commons licence, and indicating if licenced material has been modified in any way.

© 2026 Acta Bioscientia

Over the past decade or more, significant progress has been made in understanding the pathophysiology of metabolic syndrome. Both genetic predisposition and environmental factors contribute to its development, with many converging on pathways involving chronic inflammation and oxidative stress, which ultimately drive tissue injury and organ dysfunction [13-15]. This growing body of knowledge has informed current management strategies, which primarily focus on lifestyle modification alongside pharmacological interventions targeting individual components of the syndrome. However, despite these advances, the prevalence of metabolic syndrome and its associated complications including diabetes, cardiovascular disease, and stroke continues to rise [14-16] This trend underscores the need for ongoing research into more effective, accessible, and safer therapeutic options, particularly those derived from natural products and nutraceuticals.

It is in view of this that increasing attention has been directed toward the role of nutraceuticals and plant-derived phytochemicals in mitigating metabolic syndrome–related alterations. Both preclinical and clinical studies have demonstrated their potential to improve metabolic outcomes [17-23]. Interest in such compounds has been further strengthened by the documented benefits of dietary patterns such as the Mediterranean diet. Among these bioactive compounds, quercetin a naturally occurring flavonoid found in a wide range of fruits, vegetables, and plants has attracted considerable attention. Quercetin exhibits potent antioxidant, anti-inflammatory, anti-apoptotic, and free radical–scavenging [24-26]. Emerging evidence also suggest that it can modulate key metabolic pathways, improve insulin sensitivity, and correct lipid abnormalities associated with metabolic syndrome [24-26]. Additionally, experimental studies have shown its capacity to attenuate oxidative stress and inflammatory responses [17, 25]. Despite these promising findings, most studies have focused on the effects of quercetin on individual components of metabolic syndrome. Its impact on vital organs such as the liver and kidneys, particularly in the context of diet-induced metabolic syndrome, remains less well characterized. This gap in knowledge provides the rationale for the present study.

2. Materials and Methods

2.1 Chemicals and Drugs

Quercetin (500 mg, MRM Nutrition, USA), Cyclophosphamide injection (Endoxan-Asta®), normal saline; Assay kits for Alanine transaminase, aspartate transaminase), urea and creatinine were obtained from Randox Laboratories, Crumlin, Co. Antrim, UK). Assay kits for insulin, leptin, adiponectin, lipid peroxidation (malondialdehyde), interleukin-10, tumour necrosis factor alpha and total antioxidant capacity were sourced from Biovision Inc., (Milpitas, CA, USA).

2.2 Animals

Healthy male Wistar rats used in this study were obtained from the animal house of the Ladoke Akintola University of Technology Ogbomoso, Oyo State, Nigeria. Rats were housed in wooden cages. All procedures were conducted in accordance with the approved protocols of the Faculty of Basic Medical Sciences, Ladoke Akintola University of Technology and within the provisions for animal care and use prescribed in the scientific procedures on living animals, European Council Directive (EU2010/63).

2.3 Diet

All animals were maintained on commercially available standard rodent chow (29% protein, 11% fat, and 58% carbohydrate) provided *ad libitum* from weaning. At the start of the experiment, the animals were assigned to either a standard diet (SD) or a high-fat, high-sugar (HFHS) diet, formulated according to previously established protocols [19, 27, 28]. The HFHS diet consisted of approximately 40% fat and 48% carbohydrate, prepared using palm olein and hydrogenated vegetable shortening, with the addition of 25% soluble powdered sucrose to enhance sugar content.

2.4 Experimental methodology

Thirty adult male rats weighing 120-150 g each were randomly assigned into five groups (A, B C D and E) of six (n=6) animals each. Group A and B served as normal control and High–fat high-sugar diet control respectively. Rats in groups C and D were fed quercetin incorporated into HFHS diet at 100 and 200 mg/kg of feed respectively, while rats in group E were administered metformin at 25 mg/kg. Standard diet and quercetin supplemented diet were administered daily for 56 days. Body weight and food consumption were measured using a weighing balance as described in an earlier study [29]. At the end of the study, animals were fasted overnight following which blood was taken through the tail vein for the assessment of glucose levels. Animals were then euthanised and blood taken via an intracardiac puncture for estimation of plasma levels of insulin, leptin and adiponectin, as well as serum levels of urea, creatinine, alanine transaminase and aspartate transaminase levels. The liver and kidneys were removed, observed grossly, weighed following which they were either homogenised or fixed in 10% neutral buffered formalin. Supernatant from homogenised liver and kidney tissue were used to assess antioxidant status, lipid peroxidation levels and inflammatory markers, while fixed sections of the liver and kidneys were processed for general histological study.

2.5 Determination of body weight and feed intake

Daily feed intake and weekly body weight were measured using a digital balance. Relative change in food intake or body weight was calculated using the equation below.

$$\frac{\text{Final body weight (or feed intake)} - \text{Initial body weight (or feed intake)}}{\textit{Initial body weight (or feed intake)}}(g)$$

Table 1: Experimental method

Groups	Standard diet	HFHS diet	Quercetin	Metformin
A (SD)	Yes	No	No	No
B (HFHS)	No	Yes	No	No
C (HFHS/Q100)	No	Yes	Yes	No
D (HFHS/ Q200)	No	Yes	Yes	No
E (HFHS/ MET 25)	No	Yes	No	Yes

SD; Standard diet, Q: Quercetin, HFHS: High fat high sugar diet, MET: Metformin

2.6 Tissue Homogenisation

Homogenate (10%) of the liver and kidney tissue was prepared using ice-cold phosphate-buffered saline and centrifuged at 5,000 rpm (4 °C) for 15 min. The supernatant was then used for biochemical analyses.

2.7 Blood Chemistry

2.7.1 Estimation of Glucose, Insulin, Leptin and Adiponectin level

Glucose was measured using the glucose oxidase method. Plasma insulin, leptin and adiponectin levels were determined using enzyme-linked immunosorbent assay (ELISA) insulin, leptin and adiponectin kits (Biovision Inc., Milpitas, CA, USA) following the manufacturer's instructions.

2.7.2 Lipid profile

Total cholesterol, triglycerides, HDL-C, and LDL-C in serum were analysed using commercially available kits (RANDOX Laboratories, Crumlin, Co. Antrim, UK) as previously described

2.7.3 Lipid peroxidation (Malondialdehyde) levels

The lipid peroxidation kit was used to measure malondialdehyde (MDA) levels in samples by measuring the thiobarbituric acid-reactive species. Reactive substances of the thiobarbituric acid reacted with free MDA in the tissue to produce a coloured complex (TBAR-MDA adducts) which is measured at an absorbance of 532 nm. The MDA concentration is expressed as nmol/g [30].

2.7.4 Total antioxidant Capacity

The total antioxidant capacity (TAC) was determined using the direct assay (Trolox (6-hydroxy-2, 5, 7, 8-tetramethylchroman-2-carboxylic acid equivalent), which is based on the ability of antioxidants in a sample to reduce or inhibit oxidized products generated in the assay. A 2, 2'-azino-bis (3-ethylbenz-thiazoline-6-sulfonic acid radical (is form which has a blue-green color, when measured spectrophotometrically at 650-820 nm [30].

2.7.5 Inflammatory markers

Tumour necrosis factor-α, interleukin (IL)-10 and Interleukin 1 β level were measured using enzyme-linked immunosorbent assay (ELISA) techniques with commercially available kits (Biovision Inc., Milpitas, CA, USA) [25].

2.8 Histopathological examination

The liver and kidneys were dissected out and fixed in 10% formolsaline. Tissues were processed, embedded in paraffin and sectioned at 5 µm thickness. Sections of the liver and kidneys were stained with haematoxylin-eosin stain for microscopic examination. All sections were examined with a Sellon-Olympus light microscope.

2.9 Histomorphometric and Computational Image Analysis

Histomorphometric and computational image analyses were performed on representative haematoxylin and eosin (H&E)-stained liver and kidney photomicrographs obtained from 3 animals each in all experimental groups. Digital images were captured using a light microscope coupled to a high-resolution digital camera under identical illumination and magnification settings. Image acquisition was standardized to minimize variability in staining intensity and contrast between sections. Captured photomicrographs were calibrated using a spatial resolution factor of 15 µm/pixel prior to quantitative analysis. Histomorphometric analyses were conducted using automated digital image analysis workflows implemented in ImageJ/Fiji and computational image-processing algorithms. Images were converted to grayscale where appropriate, followed by Gaussian filtering and threshold segmentation to identify tissue components and cellular profiles. Quantitative morphometric parameters evaluated included cellular profile density (cells/mm^3), mean cellular area (µm^2), stained area fraction (%), vacuolation index (%), optical density, and texture entropy. Cellular profile density was estimated using connected-component segmentation analysis of thresholded tissue regions. Mean cellular area was determined from segmented cellular profiles and calibrated to square micrometers using the image scale conversion factor.

The vacuolation index was estimated as the percentage of low-density or unstained regions relative to total tissue area, representing areas of tissue rarefaction and vacuolar degeneration. Optical density was computed from grayscale intensity values using logarithmic transformation of mean pixel intensity to assess staining compactness and tissue integrity. Texture entropy analysis was performed using grayscale histogram distribution to evaluate tissue heterogeneity and structural complexity within the tissue sections. Colour histogram analysis was performed using red-green-blue (RGB) channel decomposition of the original photomicrographs. Mean red, green, and blue intensity values were extracted for each section to assess treatment-related alterations in chromatic

staining distribution and tissue staining characteristics. Comparative computational RGB histogram plots were generated to visualize intergroup variations in morphometric and staining parameters. All analyses were performed under identical thresholding and segmentation conditions to ensure consistency across experimental groups.

2.10 Statistical analysis

Data were analysed using Chris Rorden's ezANOVA for windows (version 0.98). Hypothesis was tested using analysis of variance (ANOVA). One-way ANOVA was used for analyses. Tukey's honest significant difference (HSD) test was used for within-and between-group comparisons. Results were expressed as Mean ± S.E.M, and *p* values <0.05 was considered statistically significant.

3. Result

3.1 Effect of quercetin on body weight

Figure 1 shows the effect of quercetin on body weight. There was a significant ($p < 0.001$) increase in body weight in groups fed high fat high sugar (HFHS) diet, HFHS and Quercetin (HFHS/Q) at 100 and 200 mg/kg of feed and, and administered HFHS with metformin (HFHS/MET) at 25 mg/kg body weight compared to control. Compared to HFHS control, body weight decreased significantly with HFHS/Q100 HFHS/Q200 and HFHS/MET. Compared to HFHS/MET, body weight decreased with HFHS/Q200.

3.2 Effect of quercetin on feed intake

Figure 2 shows the effect of quercetin on feed intake. There was a significant ($p < 0.001$) increase in feed intake with HFHS, HFHS/Q100, HFHS/Q200 and HFHS/MET compared to control. Compared to HFHS control, feed intake decreased significantly with HFHS/Q100 HFHS/Q200 and HFHS/MET. Compared to HFHS/MET, feed intake decreased with HFHS/Q100 and HFHS/Q200.

3.3 Effect of Quercetin on blood glucose and plasma insulin levels

Figure 3 (upper level) shows the effect of quercetin on blood glucose levels. There was a significant ($p < 0.001$] increase in blood glucose levels with HFHS, HFHS/Q100, HFHS/Q200 and HFHS/MET compared to control. Compared to HFHS control, blood glucose levels decreased significantly with HFHS/Q100 HFHS/Q200 and HFHS/MET. Compared to HFHS/MET, blood glucose levels decreased with HFHS/Q200.

Figure 3 (lower level) shows the effect of quercetin on plasma insulin levels. There was a significant ($p < 0.001$] increase in plasma insulin levels with HFHS and HFHS/MET and a decrease with HFHS/Q200 compared to control. Compared to HFHS control, plasma insulin levels decreased significantly with HFHS/Q100 HFHS/Q200 and HFHS/MET. Compared to HFHS/MET, plasma insulin decreased with HFHS/Q100 and HFHS/Q200.

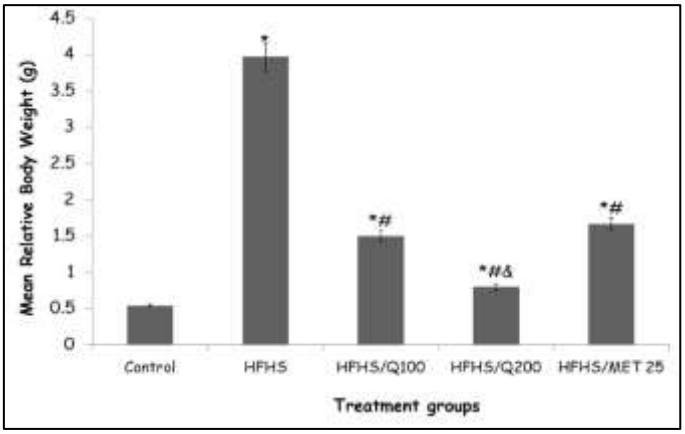


Figure 1: Effect of quercetin on body weight in rats. Each bar represents Mean ± S.E.M, $^{*}p < 0.05$ significant difference from control, $^{\#}p < 0.05$ significant difference from HFHS control, $^{\&}p < 0.05$ significant difference from HFHS/MET, number of rats per treatment group =6.

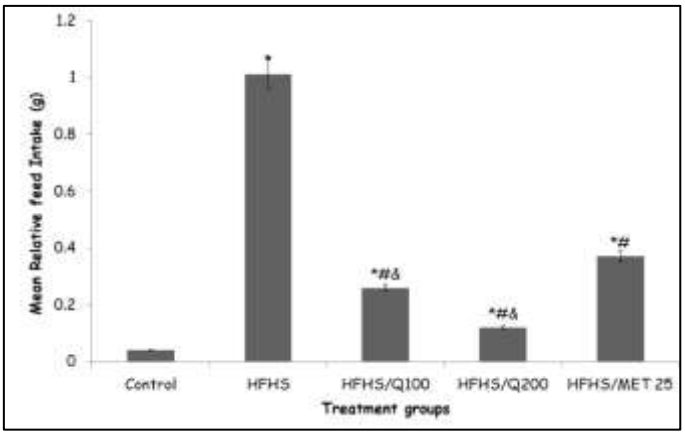


Figure 2: Effect of quercetin on feed intake in rats. Each bar represents Mean ± S.E.M, $^{*}p < 0.05$ significant difference from control, $^{\#}p < 0.05$ significant difference from HFHS control, $^{\&}p < 0.05$ significant difference from HFHS/MET, number of rats per treatment group =6

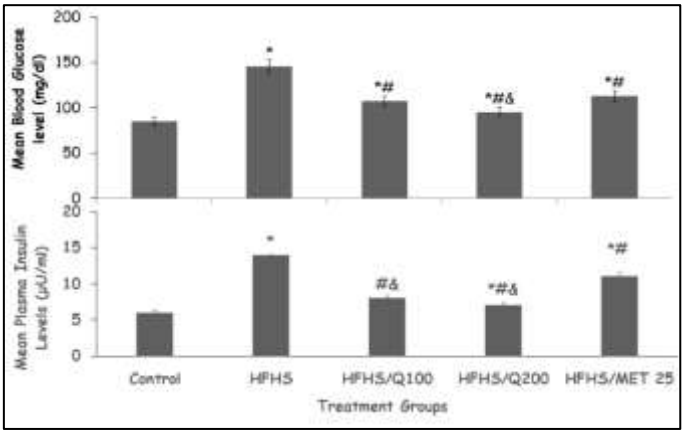


Figure 3: Effect of quercetin on blood glucose levels (Upper panel) and plasma insulin level (Lower panel) in rats. Each bar represents Mean ± S.E.M, $^{*}p < 0.05$ significant difference from control, $^{\#}p < 0.05$ significant difference from HFHS control, $^{\&}p < 0.05$ significant difference from HFHS/MET, number of rats per treatment group =6.

3.4 Effect of Quercetin on adiponectin and leptin levels

Figure 4 shows the effect of quercetin on leptin (Upper panel) and adiponectin (Lower panel) levels. There was a significant ($p < 0.001$] increase in plasma leptin levels with HFHS and HFHS/MET and a decrease with HFHS/Q200 compared to control. Compared to HFHS control, plasma leptin levels decreased significantly with HFHS/Q100 HFHS/Q200 and HFHS/MET. Compared to HFHS/MET, plasma leptin decreased with HFHS/Q200. Plasma adiponectin levels decreased significantly with HFHS, compared to control. Compared to HFHS, adiponectin levels increased with HFHS/Q100, HFHS/Q200 and HFHS/MET. Compared to HFHS/MET, adiponectin levels increased with HFHS/Q100 and HFHS/Q200.

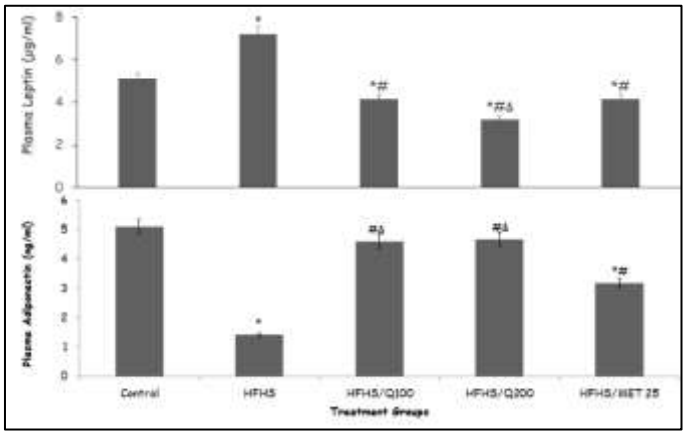


Figure 4: Effect of quercetin on leptin (Upper panel) and adiponectin (Lower panel) levels in rats. Each bar represents Mean ± S.E.M, $^{*}p < 0.05$ significant difference from control, $^{\#}p < 0.05$ significant difference from HFHS control, $^{\&}p < 0.05$ significant difference from HFHS/MET, number of rats per treatment group =6

3.5 Effect of Quercetin on biochemical parameters of liver and kidney integrity

Table 2 shows the effect of quercetin on biochemical parameters of liver and kidney integrity including urea, creatinine, alkaline phosphatase, alanine and aspartate transaminase.

Urea levels increased significantly with HFHS, and HFHS/MET and decreased with HFHS/Q100 and HFHS/Q200 compared to control. Compared to HFHS, urea levels decreased with HFHS/Q100, HFHS/Q200 and HFHS/MET. Compared to HFHS/MET, urea levels decreased with HFHS/Q100 and HFHS/Q200.

Creatinine levels increased significantly with HFHS, and HFHS/Q100 and decreased with HFHS/Q200 and HFHS/MET compared to control. Compared to HFHS, creatinine levels decreased with HFHS/Q100, HFHS/Q200 and HFHS/MET. Compared to HFHS/MET, creatinine levels increased with HFHS/Q100 and decreased with HFHS/Q200.

Alanine transaminase (ALT) and Aspartate transaminase (AST) activities increased significantly with HFHS, and decreased with HFHS/Q200 compared to control. Compared to HFHS, ALT and AST activities decreased with HFHS/Q100, HFHS/Q200 and HFHS/MET. Compared to HFHS/MET, ALT and AST activities decreased with HFHS/Q200.

Alkaline Phosphatase (ALP) levels increased significantly with HFHS, compared to control. Compared to HFHS, ALP levels decreased with HFHS/Q100, HFHS/Q200 and HFHS/MET. Compared to HFHS/MET, ALP levels did not differ significantly with either HFHS/Q100 or HFHS/Q200.

Table 2: Biochemical Parameters of Liver and Kidney Integrity

Groups	Urea mg/dl	Creatinine µmol/l	ALTU/L	ASTU/L	ALP U/L
Control	80.42±0.12	86.53±0.10	25.04±0.10	39.63±0.10	42.71±0.11
HFHS	112.44±0.11*	162.93±0.10*	65.04±0.12*	73.11±0.13*	65.55±0.12*
HFHS/Q100	71.67±0.12$^{*\#\&}$	110.13±0.11$^{*\#\&}$	30.90±0.14$^{*\#}$	52.8910.12$^{*\#}$	43.87±0.12$^{*\#}$
HFHS/Q200	70.00±0.10$^{*\#\&}$	68.67±0.11$^{*\#\&}$	17.16±0.11$^{*\#\&}$	44.7±0.11$^{*\#\&}$	42.01±0.11$^{*\#}$
HFHS/MET	95.42±0.11$^{*\#}$	70.8±0.13$^{*\#}$	32.92±0.10$^{*\#}$	58.71±0.12$^{*\#}$	44.7±0.11$^{*\#}$

Data presented as Mean ±S.E.M, $^{*}p < 0.05$ significant difference from control, $^{\#}p < 0.05$ significant difference from HFHS control, $^{\&}p < 0.05$ significant difference from HFHS/MET

3.6 Effect of Quercetin on Serum Lipid Levels

Table 3 shows the effect of quercetin on serum lipid levels. Total cholesterol (TC) increased significantly in groups HFHS, and HFHS/Q100 compared to Control. Compared to HFHS, TC decreased with HFHS/Q100, HFHS/Q200 and HFHS/MET. Compared to HFHS/MET TC increased significantly with HFHS/Q100 and HFHS/Q200.

Triglyceride (Tg) increased significantly in groups HFHS compared to Control. Compared to HFHS, Tg levels decreased with HFHS/Q100, HFHS/Q200 and HFHS/MET. Compared to HFHS/MET, Tg decreased with HFHS/Q100 and HFHS/Q200

Low density lipoprotein (LDL) levels increased with HFHS, HFHS/Q100, HFHS/Q200 and HFHS/MET compared to control. Compared to HFHS, LDL levels decreased with HFHS/Q100, HFHS/Q200 and HFHS/MET. Compared to HFHS/MET, LDL increased with HFHS/Q100 and decreased with HFHS/Q200.

High density lipoprotein (HDL) levels increased significantly with HFHS, HFHS/Q100, HFHS/Q200 and HFHS/MET compared to control. Compared to HFHS, HDL increased with HFHS/Q100, HFHS/Q200 and HFHS/MET. Compared to HFHS/MET, HDL increased with HFHS/Q100 and HFHS/Q200.

Table 3: Serum Lipid Parameters

Groups	TC (mmol/L)	TG (mmol/L)	LDL (mmol/L)	HDL (mmol/L)
Control	1.47±0.23	0.47±0.13	0.62±0.25	0.37±0.03
HFHS	9.48±0.42*	2.94±0.17*	3.66±0.35*	0.44±0.05$^{*\#}$
HFHS/Q100	6.1±0.35$^{*\#\&}$	1.14±0.17$^{*\#\&}$	3.41±0.18$^{*\#\&}$	1.28±0.08$^{*\#\&}$
HFHS/Q200	5.06±0.26$^{*\#\&}$	1.72±0.12$^{*\#\&}$	2.65±0.17$^{*\#\&}$	1.47±0.02$^{*\#\&}$
HFHS/MET	4.44±0.22$^{*\#}$	2.32±0.16$^{*\#}$	2.18±0.10$^{*\#}$	0.96±0.05$^{*\#}$

Data presented as Mean ±S.E.M, $^{*}p < 0.05$ significant difference from control, $^{\#}p < 0.05$ significant difference from HFHS control, $^{\&}p < 0.05$ significant difference from HFHS/MET.

3.7 Effect of Quercetin on Oxidative stress parameters and inflammatory cytokines

Table 4 shows the effect of quercetin on oxidative stress parameters and inflammatory cytokines. Lipid peroxidation measured as malondialdehyde (MDA) increased significantly in groups HFHS, Q100, HFHS/Q200 and HFHS/MET compared to control. Compared to HFHS, MDA levels decreased with HFHS/Q100, HFHS/Q200 and HFHS/MET. Compared to HFHS/MET, MDA levels decreased significantly with HFHS/Q100 and HFHS/Q200.

Total antioxidant capacity (TAC) decreased significantly with HFHS compared to Control. Compared to HFHS, TAC levels increased with HFHS/Q100, HFHS/Q200 and HFHS/MET. Compared to HFHS/MET, TAC increased with HFHS/Q100 and HFHS/Q200. Tumour necrosis Factor (TNF)-α levels increased with HFHS, HFHS/Q100, HFHS/Q200 and HFHS/MET compared to control. Compared to HFHS, TNF-α levels decreased with HFHS/Q100, HFHS/Q200 and HFHS/MET. Compared to HFHS/MET, TNF-α increased with HFHS/Q100 and decreased with HFHS/Q200. Interleukin-10 (IL-10) levels decreased significantly with HFHS, HFHS/Q100, HFHS/Q200 and HFHS/MET compared to control. Compared to HFHS, IL-10 increased with HFHS/Q100, HFHS/Q200 and HFHS/MET. Compared to HFHS/MET, IL-10 increased with HFHS/Q100 and HFHS/Q200.

3.8 Histopathological Evaluation of Haematoxylin and Eosin-Stained Sections of the Rat Liver

Representative photomicrographs of H&E-stained liver sections are presented in Figure 5. The control group demonstrated preserved hepatic cytoarchitecture characterized by intact hepatocyte cords, well-defined central veins, preserved sinusoidal spaces, and normal hepatocellular morphology with minimal vacuolar changes. Hepatocytes appeared polygonal with distinct nuclei and uniformly distributed cytoplasm, consistent with normal hepatic histology.

The HFHS group exhibited marked hepatic histopathological alterations characterized by hepatocellular vacuolation, distortion of hepatic cords, sinusoidal disorganization, and reduced tissue compactness. Numerous hepatocytes demonstrated cytoplasmic clearing suggestive of steatotic change, while sinusoidal spaces appeared irregular and distorted, indicating metabolic and structural hepatic injury induced by high-fat/high-sugar feeding. Treatment with quercetin attenuated these hepatic alterations in a dose-dependent manner. The HFHS/Q100 group demonstrated moderate restoration of hepatic organization with reduced vacuolar degeneration and partial preservation of sinusoidal architecture relative to the untreated HFHS group. More pronounced preservation was observed in the HFHS/Q200 group, which exhibited improved hepatocyte arrangement, reduced vacuolation, and relatively preserved hepatic cord organization.

Also, the HFHS/MET group demonstrated improved hepatic architecture relative to the HFHS group, characterized by attenuation of steatotic changes, improved tissue compactness, and restoration of hepatocellular organization. However, mild residual vacuolar changes remained evident compared with control sections. The histopathological findings indicate that HFHS feeding induced marked hepatic structural alterations consistent with steatosis and metabolic injury, while quercetin and metformin treatment ameliorated several of these abnormalities and improved hepatic tissue organization.

Table 4: Oxidative Stress and Inflammatory Cytokines

Groups	TAC (mM TE)	MDA (μM)	TNF-α (pg/ml)	IL-10 (pg/ml)
Control	18.62±0.23	2.49±0.12	15.22±1.25	15.62±1.10
HFHS	4.12±0.11*	7.25±0.11*	27.21±2.35*	4.40±1.10$^{*\#}$
HFHS/Q100	10.20±0.10$^{*\#\&}$	3.54±0.20$^{*\#\&}$	19.22±1.10$^{*\#\&}$	10.21±1.20$^{*\#\&}$
HFHS/Q200	15.16±0.16$^{*\#\&}$	4.12±0.15$^{*\#\&}$	16.25±1.20$^{*\#\&}$	12.24±1.22$^{*\#\&}$
HFHS/MET	9.10±0.10$^{*\#}$	5.02±0.10$^{*\#}$	22.10±1.10$^{*\#}$	8.60±1.15$^{*\#}$

Data presented as Mean ±S.E.M, *p < 0.05 significant difference from control, #p < 0.05 significant difference from HFHS control, &p < 0.05 significant difference from HFHS

3.7 Quantitative Histomorphometric and Colour Histogram Analysis of the Rat Liver (H&E) Analysis

Quantitative histomorphometric and RGB colour histogram analyses of H&E-stained liver sections demonstrated marked treatment-dependent alterations in hepatocellular density, cellular morphology, staining compactness, and chromatic staining characteristics across the experimental groups (Table 5). The control group demonstrated preserved hepatic structural organization characterized by 299.0 ± 22.23 cellular profiles/mm³, a mean cellular area of 44,773.49 ± 47.32 μm², and stained area fraction of 32.28 ± 2.22%. RGB histogram analysis revealed red, green, and blue mean intensity values of 219.65 ± 11.21, 108.25 ± 9.21, and 239.45 ± 9.32, respectively, reflecting balanced eosinophilic and basophilic staining patterns consistent with normal hepatocellular architecture and preserved tissue compactness.

The HFHS group demonstrated increased cellular profile density (351.0 ± 27.15 cells/mm³) together with a reduction in mean cellular area (39,739.10 ± 56.23 μm²) relative to the control group. Stained area fraction was mildly increased (33.63 ± 2.13%), while RGB histogram analysis demonstrated red, green, and blue intensity values of 221.19 ± 11.11, 101.82 ± 8.11, and 240.25 ± 7.45, respectively. These findings suggest increased hepatocellular clustering and altered tissue organization associated with HFHS-induced metabolic stress and early steatotic changes. The HFHS/Q100 group demonstrated the highest cellular profile density among all groups (367.0 ± 24.54 cells/mm³) together with a mean cellular area of 41,441.08 ± 44.23 μm² and stained area fraction of 36.67 ± 1.54%. RGB histogram analysis revealed relatively preserved red and green intensity values of 219.64 ± 10.12 and 101.10 ± 7.21, respectively, with a slightly reduced blue intensity (236.40 ± 6.88). These findings suggest partial preservation of hepatocellular organization and improved tissue compactness

following low-dose quercetin treatment. More pronounced alterations were observed in the HFHS/Q200 group, which demonstrated reduced cellular profile density (276.0 ± 23.22 cells/mm³), markedly reduced mean cellular area (24,917.93 ± 54.23 µm²), and substantially reduced stained area fraction (16.58 ± 0.54%). RGB histogram analysis revealed elevated red and green intensity values of 237.95 ± 10.11 and 167.45 ± 6.12, respectively, together with increased blue intensity (247.65 ± 8.67). These findings indicate marked disruption of staining compactness, altered hepatocellular morphology, and significant changes in hepatic tissue organization. The HFHS/MET group demonstrated the most pronounced morphometric alterations characterized by the lowest cellular profile density (173.0 ± 18.23 cells/mm³), smallest mean cellular area (15,138.73 ± 44.34 µm²), and markedly reduced stained area fraction (6.32 ± 0.01%). RGB histogram analysis demonstrated markedly elevated red, green, and blue intensity values of 246.57 ± 10.13, 203.06 ± 4.23, and 251.79 ± 6.66, respectively. These findings suggest severe alterations in staining distribution, reduced tissue compactness, and substantial disruption of hepatocellular organization. Collectively, these findings demonstrate that HFHS feeding induced significant alterations in hepatic histomorphology and staining characteristics consistent with metabolic and steatotic injury. Quercetin treatment, particularly at 100 mg/kg, partially preserved hepatocellular organization and staining compactness, while higher-dose quercetin and metformin treatment groups demonstrated more pronounced alterations in morphometric and chromatic staining parameters.

3.10 Comparative Colour Histogram Analysis (H&E)

Comparative RGB colour histogram analysis demonstrated treatment-dependent alterations in staining intensity distribution across the H&E-stained liver sections (Figure 6). The control group exhibited balanced eosinophilic and basophilic staining patterns consistent with preserved hepatic architecture and normal hepatocellular organization. HFHS treatment altered chromatic distribution patterns characterized by increased tissue heterogeneity and changes in eosinophilic staining intensity associated with steatotic and metabolic injury. Quercetin treatment partially restored RGB intensity distributions toward control values, particularly in the HFHS/Q100 group, suggesting improved preservation of tissue compactness and hepatic organization. The HFHS/Q200 and HFHS/MET groups demonstrated marked alterations in red and green channel intensities together with increased staining heterogeneity, indicating substantial disruption of hepatocellular architecture and altered staining compactness. The relatively preserved blue channel intensity across groups likely reflects maintained nuclear staining despite varying degrees of hepatic injury.

3.11 Advanced Computational Histomorphometric Analysis of H&E-Stained Liver Sections

Table 6 shows the result of advanced computational histomorphometric analysis of H &E-stained sections of the rat liver. There was marked treatment-dependent alterations in hepatic vacuolation, optical density, tissue complexity, and stained tissue fraction across the experimental groups. The control group demonstrated moderate vacuolation index (27.8 ± 3.24%), optical density of 0.209 ± 0.23, texture entropy of 4.64 ± 0.23, and stained area fraction of 32.28 ± 2.22%, consistent with preserved hepatic tissue organization and balanced staining compactness within normal liver architecture.

The HFHS group demonstrated a slight reduction in vacuolation (24.2 ± 3.22%) relative to the control group, together with mildly increased optical density (0.218 ± 0.11), increased texture entropy (4.82 ± 0.14), and stained area fraction of 33.63 ± 2.13%. The increased texture entropy observed in this group suggests greater tissue heterogeneity and structural complexity associated with HFHS-induced metabolic alterations and early hepatic remodeling. Similarly, the mild increase in optical density may reflect increased staining compactness or altered hepatocellular organization secondary to metabolic stress. The HFHS/Q100 group demonstrated vacuolation index of 25.53 ± 1.43%, optical density of 0.222 ± 0.12, texture entropy of 4.64 ± 0.12, and the highest stained area fraction among all groups (36.67 ± 1.54%). These findings suggest partial preservation of hepatic tissue integrity and improved staining compactness following low-dose quercetin treatment. The preservation of texture entropy near control values further indicates maintenance of hepatic structural organization and tissue heterogeneity

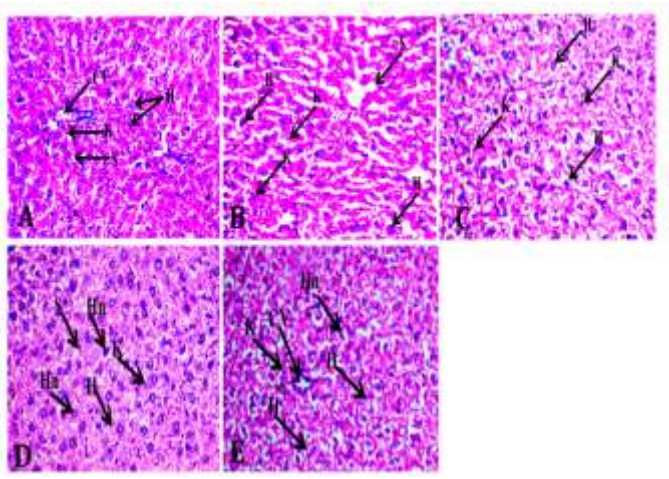


Figure 5. Representative photomicrographs of Haematoxylin and Eosin-stained liver sections across experimental groups. Representative photomicrographs showing hepatic histoarchitecture following high-fat/high-sugar (HFHS) diet induction and treatment interventions. The control group demonstrated preserved hepatic architecture with intact hepatocyte (H) cords, normal sinusoidal spaces (S), Central vein (CV), and Kupfer Cells (K), and minimal vacuolar changes. The HFHS group exhibited marked hepatocellular vacuolation, sinusoidal distortion, and disrupted hepatic organization consistent with steatotic and metabolic injury. Treatment with quercetin at 100 mg/kg (HFHS/Q100) partially restored hepatic organization with reduced vacuolar degeneration, while the HFHS/Q200 group demonstrated improved hepatocellular arrangement and reduced tissue disorganization relative to the HFHS group. Metformin-treated animals (HFHS/MET) exhibited attenuation of hepatic injury with improved tissue compactness and partial restoration of hepatic architecture. HH&E stain; scale bar = 15 µm/pixel.

Table 5: Quantitative Histomorphometric and Colour Histogram Parameters

Group	Cellular Profiles (Cells/mm³)	Mean Cellular Area (µm²)	Stained Area %	Red Mean	Green Mean	Blue Mean
Control	299.0 ±22.23	14773.49 ±47.32	32.28 ±2.22	219.65 ±11.21	108.25 ±9.21	239.4 ±9.32
HFHS	351.0 ±27.15	39739.1 ±56.23	33.63 ±2.13	221.19 ±11.11	101.82 ±8.11	240.2 ±7.45
HFHS/Q100	367.0 ±24.54	41441.08 ±44.23	36.67 ±1.54	219.64 ±10.12	101.1 ±7.21	236.4 ±6.88
HFHS/Q200	276.0 ±23.22	24917.93 ±54.23	16.58 ±0.54	237.95 ±10.11	167.45 ±6.12	247.65 ±8.67
HFHS/MET	173.0 ±18.23	15138.73 ±44.34	6.32 ±0.01	246.57 ±10.13	203.06 ±4.23	251.79 ±6.66

Values presented as mean ± S.E.M HFHS: High Fat High Sugar, Q: Quercetin, MET: Metformin, number of slides/group- 3

More pronounced alterations were observed in the HFHS/Q200 group, which demonstrated markedly increased vacuolation index (56.34 ± 2.14%), substantially reduced optical density (0.108 ± 0.12), reduced texture entropy (3.65 ± 0.13), and markedly reduced stained area fraction (16.58 ± 0.54%). These findings indicate severe disruption of hepatocellular organization, reduced tissue compactness, and loss of normal hepatic structural complexity. The marked increase in vacuolation is consistent with hepatocellular degeneration, steatotic change, and intracellular lipid accumulation, while reduced texture entropy suggests diminished tissue heterogeneity and architectural disorganization.

The HFHS/MET group demonstrated the most severe morphometric alterations among all groups, characterized by the highest vacuolation index (72.74 ± 2.54%), lowest optical density (0.059 ± 0.12), lowest texture entropy (2.70 ± 0.11), and markedly reduced stained area fraction (6.32 ± 0.01%). These findings indicate extensive hepatocellular degeneration, severe tissue rarefaction, and profound disruption of hepatic structural integrity. The markedly reduced optical density and stained area fraction suggest loss of staining compactness and diminished hepatocellular preservation, while the low texture entropy indicates marked reduction in tissue complexity and architectural organization. Together, these findings demonstrate that HFHS feeding induced progressive alterations in hepatic tissue organization and computational morphometric indices consistent with steatotic and metabolic liver injury. Low-dose quercetin treatment partially preserved tissue integrity and staining compactness, whereas the HFHS/Q200 and HFHS/MET groups demonstrated pronounced morphometric deterioration characterized by increased vacuolation, reduced optical density, diminished tissue complexity, and severe disruption of hepatic architecture.

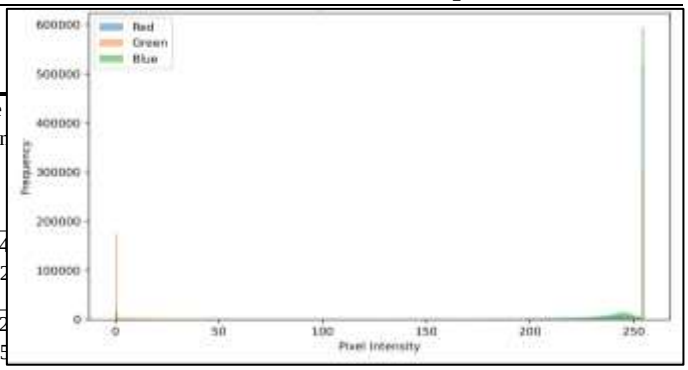


Figure 6. Comparative RGB colour histogram analysis of H&E-stained liver sections. Comparative RGB colour histogram profiles demonstrating treatment-dependent alterations in eosinophilic and basophilic staining intensity within H&E-stained liver sections following HFHS diet induction and treatment with quercetin or metformin. The control group exhibited balanced red, green, and blue intensity distributions consistent with preserved hepatic organization and intact hepatocellular morphology. HFHS treatment altered chromatic staining patterns with increased staining heterogeneity and altered eosinophilic distribution associated with steatotic injury and hepatocellular degeneration. Quercetin treatment partially restored RGB intensity distributions toward control values, particularly in the HFHS/Q100 group, indicating improved preservation of hepatic tissue organization and staining compactness. Marked alterations in red and green channel intensity observed in the HFHS/Q200 and HFHS/MET groups suggest substantial changes in hepatocellular morphology and tissue integrity.

Table 6: Advanced Computational Histomorphometric Analysis of H&E-Stained Liver Sections

Group	Vacuolation %	Optical Density	Texture Entropy	Stained Area %
Control	27.8 ±3.24	0.209±0.23	4.64±0.23	32.28 ±2.22
HFHS	24.2 ±3.22	0.218±0.11	4.82±0.14	33.63±2.13
HFHS/Q100	25.53 ±1.43	0.222±0.12	4.64 ±0.12	36.67±1.54
HFHS/Q200	56.34 ±2.14	0.108±0.12	3.65 ±0.13	16.58±0.54
HFHS/MET	72.74 ±2.54	0.059±0.12	2.70 ±0.11	6.32 ±0.01

Values presented as mean ± S.E.M HFHS: High Fat High Sugar, Q: Quercetin, MET: Metformin, number of slides/group-3

3.12 Histopathological Interpretation of Haematoxylin and Eosin (H&E)-Stained Kidney Sections

Representative photomicrographs of H&E-stained kidney sections (Figure 7) demonstrated treatment-dependent alterations in renal cortical architecture across the experimental groups. The control group exhibited preserved renal histoarchitecture characterized by intact glomeruli with well-defined Bowman's spaces, preserved tubular epithelial lining, normal interstitial organization, and minimal evidence of degenerative changes. Renal corpuscles appeared structurally intact, while proximal and distal convoluted tubules maintained normal cellular morphology and luminal organization.

The HFHS group demonstrated mild to moderate renal histopathological alterations characterized by tubular epithelial

distortion, focal vacuolar degeneration, mild glomerular congestion, and altered tubular compactness. Some renal tubules exhibited luminal irregularities and mild epithelial swelling suggestive of early metabolic and oxidative renal injury induced by high-fat/high-sugar feeding. The HFHS/Q100 group demonstrated partial preservation of renal cortical architecture relative to the HFHS group. Glomerular organization appeared relatively maintained with moderate preservation of tubular epithelial integrity. However, mild tubular distortion and focal vacuolar changes remained evident within portions of the renal cortex, indicating incomplete attenuation of HFHS-induced renal injury. More pronounced renal alterations were observed in the HFHS/Q200 group, characterized by marked tubular degeneration, extensive vacuolar changes, distortion of renal corpuscular architecture, widened interstitial spaces, and reduced tubular compactness. Several glomeruli appeared shrunken or distorted, while tubular epithelial cells demonstrated evidence of cellular degeneration and architectural disorganization. The HFHS/MET group demonstrated the most severe histopathological alterations among all groups. Renal sections exhibited extensive tubular degeneration, severe vacuolar changes, marked disruption of glomerular organization, widening of Bowman's spaces, and pronounced distortion of renal cortical architecture. Tubular epithelial integrity appeared severely compromised with substantial tissue rarefaction and loss of normal renal structural organization. Overall, the findings demonstrate that HFHS feeding induced progressive renal cortical injury characterized by tubular degeneration, vacuolar alterations, and disruption of glomerular and tubular organization. Quercetin treatment produced variable modulatory effects on renal histopathology, while the HFHS/Q200 and HFHS/MET groups demonstrated more pronounced renal structural deterioration relative to control and HFHS groups.

3.13 Quantitative Histomorphometric and Colour Histogram Analysis of H&E-Stained Kidney Sections

Quantitative histomorphometric and RGB colour histogram analyses of H&E-stained kidney sections demonstrated marked treatment-dependent alterations in renal cellular organization, staining compactness, tissue complexity, and morphometric integrity across the experimental groups (Tables 7 and 8). The control group demonstrated preserved renal cortical architecture characterized by 195.0 ± 18.22 cellular profiles/mm³, mean cellular area of 83,863.85 ± 65.21 µm², vacuolation index of 31.73 ± 2.11%, optical density of 0.213 ± 0.02, texture entropy of 4.647 ± 0.21, and stained area fraction of 39.43 ± 2.22%. RGB histogram analysis revealed red, green, and blue mean intensity values of 208.85 ± 12.11, 110.86 ± 10.22, and 243.89 ± 9.32, respectively, consistent with preserved renal tissue organization and balanced staining characteristics.

The HFHS group demonstrated increased cellular profile density (229.0 ± 20.11 cells/mm³) together with reduced mean cellular area (66,144.10 ± 54.33 µm²) relative to controls. Vacuolation index was 30.67 ± 2.14%, while optical density and texture entropy remained relatively comparable to control values. The stained area fraction was 36.52 ± 2.10%. RGB histogram analysis demonstrated increased red channel intensity (225.64 ± 13.24) together with green and blue intensities of 108.28 ± 8.43 and 250.27 ± 8.44, respectively, suggesting altered renal staining distribution associated with HFHS-induced tissue remodeling.

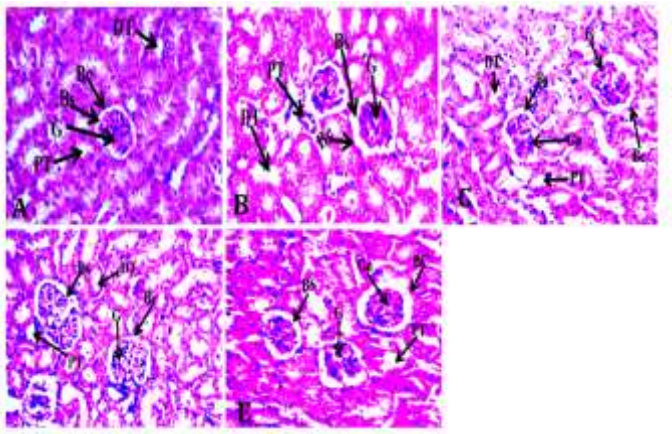


Figure 7. Representative photomicrographs of H&E-stained kidney sections across experimental groups. Representative photomicrographs showing renal cortical histoarchitecture following high-fat/high-sugar (HFHS) diet induction and treatment interventions. The control group demonstrated preserved renal architecture with intact glomeruli (Gn), Bowman's capsule(BC) well-defined Bowman's spaces (BS), and preserved tubular epithelial organization including Distal tubule(DT) and Proximal Tubule (PT). The HFHS group exhibited mild to moderate renal alterations characterized by tubular distortion, vacuolar degeneration, and altered glomerular organization. The HFHS/Q100 group demonstrated partial preservation of renal cortical architecture with moderate restoration of tubular integrity and reduced degenerative changes relative to the HFHS group. More pronounced renal alterations including tubular degeneration, widened interstitial spaces, and disrupted renal corpuscular organization were observed in the HFHS/Q200 group. The HFHS/MET group demonstrated extensive renal cortical disruption characterized by severe tubular degeneration, vacuolar changes, and marked distortion of glomerular and tubular architecture. H&E stain; scale calibration = 15 µm/pixel.

The HFHS/Q100 group demonstrated reduced cellular profile density (177.0 ± 16.23 cells/mm³) with the largest mean cellular area among all groups (87,175.42 ± 72.12 µm²). Vacuolation index increased moderately to 34.53 ± 2.33%, while optical density was 0.196 ± 0.02 and texture entropy was 4.254 ± 0.14. Stained area fraction remained relatively preserved (37.21 ± 2.01%). RGB histogram analysis demonstrated red, green, and blue mean intensity values of 232.34 ± 14.21, 108.62 ± 8.55, and 247.17 ± 8.12, respectively, indicating moderate alterations in staining distribution and renal tissue organization.

More pronounced renal morphometric alterations were observed in the HFHS/Q200 group, characterized by reduced cellular profile density (188.0 ± 17.21 cells/mm³), markedly reduced mean cellular area (39,025.53 ± 48.23 µm²), and

substantially increased vacuolation index (58.98 ± 3.12%). Optical density and texture entropy were markedly reduced to 0.101 ± 0.01 and 3.195 ± 0.12, respectively, while stained area fraction declined to 17.69 ± 1.11%. RGB histogram analysis demonstrated markedly elevated red and green channel intensities of 242.11 ± 12.44 and 170.24 ± 11.11, respectively, together with blue intensity of 251.68 ± 7.65, indicating severe disruption of staining distribution and renal tissue organization. The HFHS/MET group demonstrated the most severe morphometric alterations among all groups, characterized by the lowest cellular profile density (176.0 ± 15.34 cells/mm³), smallest mean cellular area (22,148.44 ± 44.32 µm²), highest vacuolation index (72.54 ± 3.44%), lowest optical density (0.063 ± 0.01), and lowest texture entropy (2.338 ± 0.10). Stained area fraction was markedly reduced to 9.40 ± 0.54%. RGB histogram analysis demonstrated markedly elevated red, green, and blue intensity values of 244.53 ± 11.65, 200.89 ± 12.23, and 251.76 ± 7.54, respectively, reflecting marked alterations in staining distribution and renal cytoarchitecture. Together, these findings demonstrate that HFHS feeding induced progressive renal structural alterations characterized by altered cellular organization, reduced tissue compactness, and disruption of renal cytoarchitecture. Quercetin treatment produced variable effects on renal morphometric indices, while the HFHS/Q200 and HFHS/MET groups demonstrated the most pronounced deterioration in tissue integrity and staining characteristics.

3.14 Comparative Colour Histogram Analysis of Haematoxylin and Eosin-stained Section of the Rat Kidney

Figure 8 demonstrates the comparative RGB colour histogram profiles of H&E-stained kidney sections across the experimental groups, revealing treatment-dependent alterations in staining intensity distribution and renal tissue organization. The control group exhibited relatively balanced red, green, and blue channel distributions, consistent with preserved renal cortical architecture, intact tubular epithelial organization, and normal eosinophilic-basophilic staining balance. The moderate red and green channel intensities together with stable blue channel distribution reflect preserved cytoplasmic and nuclear staining characteristics within normal renal tissue.

The HFHS group demonstrated mild alterations in chromatic distribution characterized by increased red channel intensity and subtle shifts in green channel distribution relative to the control group. These changes suggest early disruption of renal staining compactness and altered tissue organization associated with HFHS-induced metabolic stress and renal remodeling. The HFHS/Q100 group demonstrated histogram profiles relatively comparable to the HFHS group, with moderate preservation of chromatic distribution patterns. The relatively stable green and blue channel intensities suggest partial maintenance of renal staining organization and tissue compactness following low-dose quercetin treatment. More pronounced alterations were observed in the HFHS/Q200 group, which demonstrated marked elevation of red and green channel intensities together with broader histogram distribution patterns. These changes indicate substantial disruption of renal tissue organization, altered staining compactness, and increased heterogeneity within the renal cortex. The HFHS/MET group demonstrated the most marked chromatic alterations among all groups, characterized by the highest red and green channel intensities and pronounced rightward histogram shifts. These findings reflect severe disruption of renal staining characteristics, reduced tissue compactness, and extensive distortion of renal cytoarchitecture. The RGB histogram profiles demonstrate progressive treatment-dependent alterations in renal staining distribution and tissue organization, with the HFHS/Q200 and HFHS/MET groups exhibiting the greatest deviations from the normal chromatic patterns observed in the control group

Table 7. Histomorphometric and Colour Histogram Parameters of H&E-Stained Kidney Sections

Groups	Cellular Profiles (Cells/mm³)	Mean Cellular Area (µm²)	Red Mean	Green Mean	Blue Mean
Control	195.0 ± 18.22	83863.85 ± 65.21	208.85 ±12.11	110.86 ±10.22	243.89 ± 9.32
HFHS	229.0 ± 20.11	66144.10 ± 54.33	225.64 ±13.24	108.28 ± 8.43	250.27 ± 8.44
HFHS/Q100	177.0 ± 16.23	87175.42 ± 72.12	232.34 ±14.21	108.62 ± 8.55	247.17 ± 8.12
HFHS/Q200	188.0 ±17.21	39025.53 ± 48.23	242.11 ±12.44	170.24 ±11.11	251.68 ± 7.65
HFHS/MET	176.0 ± 15.34	22148.44 ± 44.32	244.53 ±11.65	200.89 ±12.23	251.76 ± 7.54

Values presented as mean ± S.E.M HFHS: High Fat High Sugar, Q: Quercetin, MET: Metformin, number of slides/group-3

Table 8. Advanced Computational Histomorphometric Parameters of H&E-Stained Kidney Sections

Groups	Vacuolation (%)	Optical Density	Texture Entropy	Stained Area (%)
Control	31.73 ± 2.11	0.213 ± 0.02	4.647 ± 0.21	39.43 ± 2.22
HFHS	30.67 ± 2.14	0.201 ± 0.01	4.645 ± 0.18	36.52 ± 2.10
HFHS/Q100	34.53 ± 2.33	0.196 ± 0.02	4.254 ± 0.14	37.21 ± 2.01
HFHS/Q200	58.98 ± 3.12	0.101 ± 0.01	3.195 ± 0.12	17.69 ± 1.11
HFHS/MET	72.54 ± 3.44	0.063 ± 0.01	2.338 ± 0.10	9.40 ± 0.54

Values presented as mean ± S.E.M HFHS: High Fat High Sugar, Q: Quercetin, MET: Metformin, number of slides/group-3

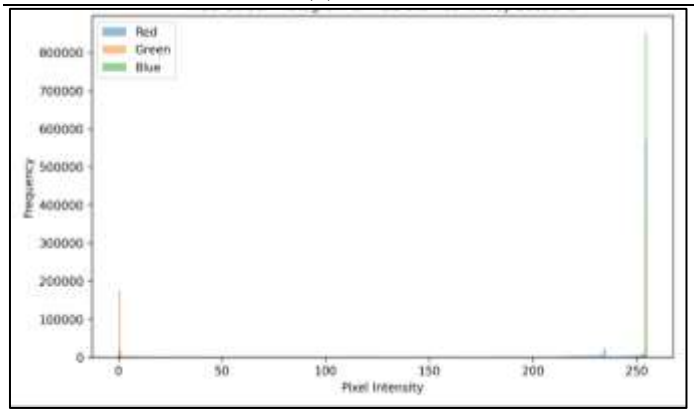


Figure 8. Comparative RGB colour histogram analysis of H&E-stained kidney sections. Comparative RGB colour histogram profiles demonstrating treatment-dependent alterations in eosinophilic and basophilic staining intensity within H&E-stained kidney sections following HFHS diet induction and treatment with quercetin or metformin. The control group exhibited balanced red, green, and blue intensity distributions consistent with preserved renal tissue organization and intact staining compactness. HFHS treatment altered chromatic staining distribution associated with renal structural remodeling and tissue injury. The HFHS/Q100 group demonstrated moderate preservation of RGB intensity patterns relative to the HFHS group, while the HFHS/Q200 and HFHS/MET groups exhibited marked elevations in red and green channel intensities together with altered staining distribution, indicating substantial disruption of renal cytoarchitecture and tissue organization.

Discussion

Metabolic syndrome is a multifactorial metabolic disorder characterized by interconnected abnormalities including obesity, insulin resistance, dyslipidemia, hyperglycemia, oxidative stress, and chronic low-grade inflammation, all of which significantly increase the risk of cardiovascular, hepatic, and renal diseases [3, 4, 13, 28, 31]. Experimental induction of metabolic syndrome using a high-fat/high-sugar (HFHS) diet has been shown to reproduce many of these metabolic and pathological disturbances in rodents, including altered glucose metabolism, dyslipidaemia, inflammation, oxidative stress, and organ dysfunction [27, 32].

In the present study, HFHS feeding produced significant increases in body weight and feed intake relative to control animals, confirming successful induction of metabolic syndrome. These findings are consistent with previous reports demonstrating that excessive dietary fat and sugar intake promotes hyperphagia, increased adiposity, and metabolic imbalance [33, 34]. Quercetin, treatment on the other hand treatment, especially at 200 mg/kg, significantly reduced both body weight and feed intake relative to untreated HFHS animals, suggesting modulation of appetite regulation, energy utilization, and metabolic efficiency [17, 24-26]. These findings support reports demonstrating that quercetin improves metabolic homeostasis and attenuates diet-induced obesity through regulation of lipid metabolism and insulin signaling pathways [35, 36].

HFHS feeding also produced marked hyperglycemia and hyperinsulinemia, indicating impaired glucose tolerance and insulin resistance. Elevated plasma insulin levels in the HFHS group likely reflect compensatory pancreatic β-cell activity secondary to peripheral insulin resistance. Quercetin treatment significantly reduced blood glucose and plasma insulin levels relative to untreated HFHS animals, particularly in the HFHS/Q200 group. These findings support earlier reports demonstrating that quercetin enhances glucose uptake, improves insulin sensitivity, suppresses oxidative stress, and regulates signaling pathways involved in glucose metabolism. The reduction in circulating insulin following quercetin treatment may indicate improved peripheral insulin responsiveness and reduced metabolic burden on pancreatic β-cells [35, 36]. Studies have also demonstrated that hypercaloric diets like HFHS diets have the ability to alter satiety signaling through the uncoupling of hypothalamic oxytocin neurons which reduces the brain's response to gut-derived satiety hormones, causing overeating and snacking behaviours [37].

In this study adipokine analysis further supported the presence of HFHS-induced metabolic dysregulation. HFHS feeding significantly increased plasma leptin levels while reducing adiponectin concentrations relative to controls. Elevated leptin levels are commonly associated with increased adiposity and leptin resistance, whereas reduced adiponectin is linked to impaired insulin sensitivity, inflammation, and metabolic dysfunction. Quercetin treatment reversed many of these alterations, particularly at higher doses, suggesting improvement in adipose tissue signaling and metabolic regulation. Increased adiponectin levels following quercetin administration may contribute to improved insulin sensitivity, enhanced lipid metabolism, and reduced inflammatory activity [35-73].

The lipid profile findings further confirmed significant metabolic disturbance following HFHS feeding. Marked increases in total cholesterol, triglycerides, and LDL levels were observed in HFHS-fed animals, indicating severe dyslipidemia [36]. These findings are consistent with previous studies demonstrating that HFHS diets disrupt lipid homeostasis through enhanced hepatic lipogenesis, impaired lipid clearance, and increased lipid peroxidation. Quercetin treatment significantly reduced total cholesterol, triglycerides, and LDL concentrations while increasing HDL levels relative to untreated HFHS animals. These observations suggest that quercetin may improve lipid metabolism through inhibition of hepatic cholesterol synthesis, enhancement of lipid clearance, and reduction of oxidative lipid damage. The beneficial effects of quercetin on lipid metabolism have been widely attributed to its antioxidant and anti-inflammatory properties, as well as modulation of genes involved in lipid transport and metabolism [36, 38]. Assessment of oxidative stress and inflammatory

cytokines further demonstrated profound metabolic injury following HFHS feeding. Increased malondialdehyde (MDA) levels in HFHS animals indicate enhanced lipid peroxidation and oxidative membrane damage, while reduced total antioxidant capacity (TAC) suggests depletion of endogenous antioxidant defenses. Elevated TNF-α levels together with reduced IL-10 concentrations further confirm the presence of chronic inflammatory activation associated with metabolic syndrome. Quercetin treatment significantly reduced MDA and TNF-α levels while increasing TAC and IL-10 concentrations relative to untreated HFHS animals. These findings strongly support the antioxidant and anti-inflammatory effects of quercetin [38, 39]. Quercetin is known to scavenge reactive oxygen species, enhance endogenous antioxidant enzyme activity, suppress NF-κB activation, and inhibit pro-inflammatory cytokine release, thereby attenuating oxidative and inflammatory tissue injury [40].

Biochemical markers of hepatic and renal integrity demonstrated substantial organ dysfunction following HFHS feeding. Significant elevations in ALT, AST, and ALP activities in HFHS animals indicate hepatocellular injury and impaired hepatic membrane integrity [41]. Similarly, elevated urea and creatinine levels suggest renal functional impairment and reduced glomerular filtration efficiency. Quercetin treatment significantly reduced liver enzyme activities as well as urea and creatinine levels, particularly in the HFHS/Q200 group, suggesting preservation of hepatic and renal function. These protective effects may be attributed to attenuation of oxidative stress, stabilization of cellular membranes, and reduction of inflammatory-mediated tissue injury [42].

Histopathological examination of liver sections demonstrated that HFHS feeding disrupted normal hepatic cytoarchitecture, characterized by hepatocellular vacuolation, sinusoidal distortion, altered hepatocyte arrangement, and reduced tissue compactness. These findings are characteristic of hepatic steatosis and metabolic liver injury associated with excessive lipid accumulation, oxidative stress, mitochondrial dysfunction, and inflammatory activation. Quantitative histomorphometric analysis further supported these observations, as the HFHS group demonstrated altered cellular profile density and morphometric organization consistent with hepatic tissue remodeling secondary to metabolic stress. The HFHS/Q100 group demonstrated partial preservation of hepatic architecture with relatively preserved staining compactness and tissue organization. The preservation of chromatic staining patterns and morphometric indices in this group suggests that low-dose quercetin may attenuate oxidative stress and stabilize hepatocellular integrity through its antioxidant and anti-inflammatory actions. Previous studies have similarly demonstrated that quercetin protects against hepatic injury induced by endotoxins, ethanol, aflatoxins, and other hepatotoxic insults through suppression of oxidative damage and enhancement of endogenous antioxidant defenses [43]. In contrast, the HFHS/Q200 and HFHS/MET groups demonstrated more pronounced hepatic morphometric alterations characterized by increased vacuolation, reduced staining compactness, altered histogram distributions, and reduced tissue complexity. These findings suggest substantial disruption of hepatocellular organization and hepatic tissue integrity. The elevated red and green histogram intensities observed in these groups further support significant alterations in staining distribution and hepatocellular architecture.

Renal histopathological findings demonstrated that HFHS feeding also induced significant renal cortical injury characterized by tubular epithelial distortion, vacuolar degeneration, altered glomerular organization, and widening of interstitial spaces. These observations are consistent with previous reports indicating that metabolic syndrome promotes renal oxidative stress, glomerular dysfunction, tubular degeneration, and inflammatory injury [44, 45]. Quantitative renal morphometric analysis demonstrated altered cellular organization and morphometric remodeling within the renal cortex of HFHS-fed animals. The HFHS/Q100 group demonstrated partial preservation of renal structural organization and staining characteristics, suggesting that lower-dose quercetin exerted modest renoprotective effects through preservation of tubular epithelial integrity and attenuation of oxidative stress-mediated injury. However, the HFHS/Q200 and HFHS/MET groups demonstrated severe renal morphometric deterioration characterized by extensive tubular degeneration, altered glomerular architecture, increased vacuolar changes, and severe disruption of renal tissue organization. Colour histogram analysis further demonstrated marked alterations in staining distribution within these groups, reflecting substantial disruption of renal cytoarchitecture and tissue integrity.

The combined hepatic and renal findings suggest that HFHS feeding induced systemic metabolic injury affecting multiple organs through mechanisms involving oxidative stress, lipid dysregulation, mitochondrial dysfunction, chronic inflammation, and altered tissue organization. Both liver and kidney tissues demonstrated treatment-dependent alterations in cellular organization, staining characteristics, and structural complexity. Low-dose quercetin appeared more protective than higher-dose quercetin in several morphometric parameters despite the biochemical improvements observed at higher doses. This observation may reflect a dose-dependent biphasic effect of quercetin. Although quercetin possesses potent antioxidant properties at moderate concentrations, higher doses may under certain conditions exhibit pro-oxidant activity capable of exacerbating cellular stress and tissue injury. Variations in tissue metabolism, intracellular accumulation, and

local oxidative burden may also contribute to these differential dose-dependent responses.

Advanced computational morphometric analyses provided additional objective evidence of tissue injury and remodeling. Alterations in optical density, texture entropy, stained area fraction, and RGB histogram distributions across severely affected groups further support the histopathological evidence of altered tissue organization and degeneration. These computational approaches complement conventional histopathology by providing quantitative assessment of tissue heterogeneity, staining compactness, and structural integrity. Overall, the combined biochemical, histopathological, histomorphometric, computational, and colour histogram findings demonstrate that HFHS feeding induced significant hepatic and renal structural alterations consistent with systemic metabolic injury. Quercetin exerted significant metabolic, antioxidant, anti-inflammatory, hepatoprotective, and renoprotective effects, with low-dose quercetin demonstrating greater preservation of tissue architecture and morphometric integrity in several parameters. The study further highlights the usefulness of integrating conventional histopathology with advanced computational histomorphometric approaches for comprehensive assessment of metabolic tissue injury and therapeutic response.

Conclusion

High-fat/high-sugar (HFHS) diet-induced metabolic syndrome produced significant metabolic, hepatic, and renal alterations characterized by hyperglycemia, dyslipidemia, oxidative stress, inflammation, and structural tissue degeneration. Histopathological and computational histomorphometric analyses demonstrated marked disruption of hepatic and renal architecture, altered cellular organization, and changes in staining characteristics following HFHS feeding. Quercetin treatment improved metabolic, oxidative, inflammatory, and biochemical parameters while partially preserving hepatic and renal tissue integrity. Lower-dose quercetin demonstrated greater preservation of tissue organization in several morphometric parameters, suggesting possible dose-dependent effects. Overall, the findings indicate that quercetin exerts hepatoprotective and renoprotective effects against HFHS-induced metabolic injury and highlight the value of combining conventional histopathology with computational histomorphometric and colour histogram analyses for objective assessment of tissue injury and therapeutic response.

Funding.

None

Availability of data and materials

Data generated during and analysed during the course of this study are available from the corresponding author on request.

Competing interests

All authors of this paper declare that there is no conflict of interest related to the content of this manuscript.

Received: 11th April, 2026, Revised 24th May, 2026, Accepted: 6th June, 2025, **Published online:25/06/26**

References

1. Swarup S, Ahmed I, Grigorova Y, et al. Metabolic Syndrome. [Updated 2024 Mar 7]. In: StatPearls [Internet]. Treasure Island (FL): StatPearls Publishing; 2026 Jan-. Available from: https://www.ncbi.nlm.nih.gov/books/NBK459248/
2. Thomaz FS, John OD, Sinha P, Shafie SR, Worrall S. The Metabolic Syndrome: An Overview and Proposed Mechanisms. *Obesities*. 2024; 4(3):226-255. https://doi.org/10.3390/obesities4030020
3. Onaolapo AY, Onaolapo OJ. Nutraceuticals and diet-based phytochemicals in type 2 diabetes mellitus: from whole food to components with defined roles and mechanisms. Current Diabetes Reviews. 2020 Jan 1;16(1):12-25.
4. Onaolapo AY, Ojo FO, Adeleye OO, Falade J, Onaolapo OJ. Diabetes mellitus and energy dysmetabolism in Alzheimer's disease: understanding the relationships and potential therapeutic targets. Current Diabetes Reviews. 2023 Oct 1;19(8):31-45.
5. Jamali Z, Ayoobi F, Jalali Z, Bidaki R, Lotfi MA, Esmaeili-Nadimi A, Khalili P. Metabolic syndrome: a population-based study of prevalence and risk factors. Sci Rep. 2024 Feb 17;14(1):3987. doi: 10.1038/s41598-024-54367-4. PMID: 38368464; PMCID: PMC10874377.
6. Siam NH, Snigdha NN, Tabasumma N, Parvin I. Diabetes Mellitus and Cardiovascular Disease: Exploring Epidemiology, Pathophysiology, and Treatment Strategies. Rev Cardiovasc Med. 2024 Dec 11;25(12):436. doi: 10.31083/j.rcm2512436.
7. Sharma, A., Mittal, S., Aggarwal, R. *et al.* Diabetes and cardiovascular disease: inter-relation of risk factors and treatment. *Futur J Pharm Sci* **6**, 130 (2020). https://doi.org/10.1186/s43094-020-00151-w
8. Li, Y., Liu, Y., Liu, S. *et al.* Diabetic vascular diseases: molecular mechanisms and therapeutic strategies. *Sig Transduct Target Ther* **8**, 152 (2023). https://doi.org/10.1038/s41392-023-01400-z
9. Amirkalali B, Fakhrzadeh H, Sharifi F, Kelishadi R, Zamani F, Asayesh H, Safiri S, Samavat T, Qorbani M. Prevalence of Metabolic Syndrome and Its Components in the Iranian Adult Population: A Systematic Review and Meta-Analysis. Iran Red Crescent Med J. 2015 Dec 27;17(12):e24723. doi: 10.5812/ircmj.24723.
10. World Health Organization. Implementation road map 2023-2030 for the Global Action [lan for the prevention and control of non-communicable diseases: 2013-2030. https://www.who.int/teams/noncommunicable-diseases/governance/roadmap Accessed on April 25 2026.
11. Ranasinghe P, Mathangasinghe Y, Jayawardena R, Hills AP, Misra A. Prevalence and trends of metabolic syndrome among adults in the asia-pacific region: a systematic review. BMC Public Health. 2017, 17(101) https://doi.org/10.1186/s12889-017-4041-1
12. Onaolapo AY, Onaolapo OJ. Herbal beverages and brain function in health and disease. InFunctional and medicinal beverages 2019 Jan 1 (pp. 313-349). Academic Press.
13. Masenga SK, Kabwe LS, Chakulya M, Kirabo A. Mechanisms of Oxidative Stress in Metabolic Syndrome. Int J Mol Sci. 2023 Apr 26;24(9):7898. doi: 10.3390/ijms24097898.
14. Rochlani Y, Pothineni NV, Kovelamudi S, Mehta JL. Metabolic syndrome: pathophysiology, management, and modulation by natural compounds. Ther Adv Cardiovasc Dis. 2017 Aug;11(8):215-225. doi: 10.1177/1753944717711379..
15. Fahed G, Aoun L, Bou Zerdan M, Allam S, Bou Zerdan M, Bouferraa Y, Assi HI. Metabolic Syndrome: Updates on Pathophysiology and Management in 2021. *International Journal of Molecular Sciences*. 2022; 23(2):786. https://doi.org/10.3390/ijms23020786
16. Onaolapo AY, Onaolapo OJ. Circadian dysrhythmia-linked diabetes mellitus: Examining melatonin's roles in prophylaxis and management. World J Diabetes. 2018 Jul 15;9(7):99-114. doi: 10.4239/wjd.v9.i7.99.

17. Hosseini A, Razavi BM, Banach M, Hosseinzadeh H. Quercetin and metabolic syndrome: A review. Phytother Res. 2021 Oct;35(10):5352-5364. doi: 10.1002/ptr.7144. Epub 2021 Jun 8. PMID: 34101925.
18. Olofinnade AT, Onaolapo AY, Onaolapo OJ, Olowe OA, Mollica A, Zengin G, Stefanucci A. Corylus avellana L. modulates neurobehaviour and brain chemistry following high-fat diet. Frontiers in Bioscience (Landmark Edition). 2021 Jan 1;26(3):537-51.
19. Olofinnade AT, Alawode A, Onaolapo AY, Onaolapo OJ. Lepidium meyenii Supplemented Diet Modulates Neurobehavioral and Biochemical Parameters in Mice Fed High-Fat High-Sugar Diet. Endocr Metab Immune Disord Drug Targets. 2021;21(7):1333-1343. doi: 10.2174/1871530320666200821155005. PMID: 32955007.
20. Mohamed SM, Shalaby MA, El-Shiekh RA, Bakr AF, Kamel S, Emam SR, El-Banna HA. Maca roots: A potential therapeutic in the management of metabolic disorders through the modulation of metabolic biochemical markers in rats fed high-fat high-carbohydrate diet. J Ethnopharmacol. 2024 Mar 1;321:117533. doi: 10.1016/j.jep.2023.117533. Epub 2023 Dec 8. PMID: 38056538.
21. Dludla PV, Orlando P, Silvestri S, Marcheggiani F, Cirilli I, Nyambuya TM, Mxinwa V, Mokgalaboni K, Nkambule BB, Johnson R, Mazibuko-Mbeje SE, Muller CJF, Louw J, Tiano L. Coenzyme Q_{10} Supplementation Improves Adipokine Levels and Alleviates Inflammation and Lipid Peroxidation in Conditions of Metabolic Syndrome: A Meta-Analysis of Randomized Controlled Trials. Int J Mol Sci. 2020 May 4;21(9):3247. doi: 10.3390/ijms21093247. PMID: 32375340; PMCID: PMC7247332.
22. Genario R, Cipolla-Neto J, Bueno AA, Santos HO. Melatonin supplementation in the management of obesity and obesity-associated disorders: A review of physiological mechanisms and clinical applications. Pharmacol Res. 2021 Jan;163:105254. doi: 10.1016/j.phrs.2020.105254. Epub 2020 Oct 17. PMID: 33080320.
23. Mahdian D, Abbaszadeh-Goudarzi K, Raoofi A, Dadashizadeh G, Abroudi M, Zarepour E, Hosseinzadeh H. Effect of *Boswellia* species on the metabolic syndrome: A review. Iran J Basic Med Sci. 2020 Nov;23(11):1374-1381. doi: 10.22038/ijbms.2020.42115.9957.
24. Carrillo-Martinez EJ, Flores-Hernández FY, Salazar-Montes AM, Nario-Chaidez HF, Hernández-Ortega LD. Quercetin, a Flavonoid with Great Pharmacological Capacity. *Molecules*. 2024; 29(5):1000. https://doi.org/10.3390/molecules29051000
25. Onaolapo AY, Ojo FO, Onaolapo OJ. Biflavonoid quercetin protects against cyclophosphamide-induced organ toxicities via modulation of inflammatory cytokines, brain neurotransmitters, and astrocyte immunoreactivity. Food Chem Toxicol. 2023 Aug;178:113879. doi: 10.1016/j.fct.2023.113879. Epub 2023 Jun 8. PMID: 37301500.
26. Anand David AV, Arulmoli R, Parasuraman S. Overviews of Biological Importance of Quercetin: A Bioactive Flavonoid. Pharmacogn Rev. 2016 Jul-Dec;10(20):84-89. doi: 10.4103/0973-7847.194044. PMID: 28082789; PMCID: PMC5214562.
27. Onaolapo OJ, Omotoso SA, Olofinnade AT, Onaolapo AY. Anti-Inflammatory, Anti-Oxidant, and Anti-Lipaemic Effects of Daily Dietary Coenzyme-Q10 Supplement in a Mouse Model of Metabolic Syndrome. Antiinflamm Antiallergy Agents Med Chem. 2021;20(4):380-388. doi: 10.2174/1871523020666210427111328.
28. Onaolapo AY, Adebisi EO, Adeleye AE, Olofinnade AT, Onaolapo OJ. Dietary Melatonin Protects Against Behavioural, Metabolic, Oxidative, and Organ Morphological Changes in Mice that are Fed High-Fat, High-Sugar Diet. Endocr Metab Immune Disord Drug Targets. 2020;20(4):570-583. doi: 10.2174/1871530319666191009161228. PMID: 32138638.
29. Onaolapo AY, Onaolapo OJ, Nwoha PU Alterations in behaviour, cerebral cortical morphology and cerebral oxidative stress markers following aspartame ingestion. Journal of Chemical Neuroanatomy. 2016, 78, 42-56.
30. Falade, J., Onaolapo, A.Y. and Onaolapo, O.J., 2021. Evaluation of the behavioural, antioxidative and histomorphological effects of folic acid-supplemented diet in dexamethasone-induced depression in mice. *Central Nervous System Agents in Medicinal Chemistry (Formerly Current Medicinal Chemistry-Central Nervous System Agents)*, *21*(1), pp.73-81.
31. Dhondge RH, Agrawal S, Patil R, Kadu A, Kothari M. A Comprehensive Review of Metabolic Syndrome and Its Role in Cardiovascular Disease and Type 2 Diabetes Mellitus: Mechanisms, Risk Factors, and Management. Cureus. 2024 Aug 21;16(8):e67428. doi: 10.7759/cureus.67428.
32. Moreno-Fernández S, Garcés-Rimón M, Vera G, Astier J, Landrier JF, Miguel M. High Fat/High Glucose Diet Induces Metabolic Syndrome in an Experimental Rat Model. Nutrients. 2018 Oct 14;10(10):1502. doi: 10.3390/nu10101502.
33. Matias AM, Estevam WM, Coelho PM, Haese D, Kobi JBBS, Lima-Leopoldo AP, Leopoldo AS. Differential Effects of High Sugar, High Lard or a Combination of Both on Nutritional, Hormonal and Cardiovascular Metabolic Profiles of Rodents. Nutrients. 2018 Aug 11;10(8):1071. doi: 10.3390/nu10081071.
34. Melo BF, Sacramento JF, Ribeiro MJ, Prego CS, Correia MC, Coelho JC, Cunha-Guimaraes JP, Rodrigues T, Martins IB, Guarino MP, Seiça RM, Matafome P, Conde SV. Evaluating the Impact of Different Hypercaloric Diets on Weight Gain, Insulin Resistance, Glucose Intolerance, and its Comorbidities in Rats. Nutrients. 2019 May 28;11(6):1197. doi: 10.3390/nu11061197.
35. Jiang H, Horiuchi Y, Hironao KY, Kitakaze T, Yamashita Y, Ashida H. Prevention effect of quercetin and its glycosides on obesity and hyperglycemia through activating AMPKα in high-fat diet-fed ICR mice. J Clin Biochem Nutr. 2020 Jul;67(1):74-83. doi: 10.3164/jcbn.20-47.
36. Wang Y, Li Z, He J, Zhao Y. Quercetin Regulates Lipid Metabolism and Fat Accumulation by Regulating Inflammatory Responses and Glycometabolism Pathways: A Review. Nutrients. 2024 Apr 9;16(8):1102. doi: 10.3390/nu16081102.
37. Gruber T, Lechner F, Murat C, Contreras RE, Sanchez-Quant E, Miok V, Makris K, Le Thuc O, González-García I, García-Clave E, Althammer F, Krabichler Q, DeCamp LM, Jones RG, Lutter D, Williams RH, Pfluger PT, Müller TD, Woods SC, Pospisilik JA, Martinez-Jimenez CP, Tschöp MH, Grinevich V, García-Cáceres C. High-calorie diets uncouple hypothalamic oxytocin neurons from a gut-to-brain satiation pathway via κ-opioid signaling. Cell Rep. 2023 Oct 31;42(10):113305. doi: 10.1016/j.celrep.2023.113305.
38. Jiang L, Yi R, Chen H, Wu S. Quercetin alleviates metabolic-associated fatty liver disease by tuning hepatic lipid metabolism, oxidative stress and inflammation. Anim Biotechnol. 2025 Dec;36(1):2442351. doi: 10.1080/10495398.2024.2442351.
39. Ozorowski M, Wiciński M, Kuźmiński O, Wojciechowski P, Siedlecki Z, Śniegocki M, Włodarczyk E. The Effects of Quercetin on Vascular Endothelium, Inflammation, Cardiovascular Disease and Lipid Metabolism-A Review. Nutrients. 2025 May 3;17(9):1579. doi: 10.3390/nu17091579.
40. Wang Z, Wang P, Zhou Y, Wang L, Zhuang S. Quercetin Attenuates Oxidative Stress and Immune Inflammation via Modulating Heme and ROS Pathways in Rats Fed Protein-Oxidized Soybean Meal. Antioxidants (Basel). 2026 Apr 18;15(4):504. doi: 10.3390/antiox15040504.
41. Olofinnade AT, Onaolapo AY, Stefanucci A, Mollica A, Olowe OA, Onaolapo OJ. Cucumeropsis mannii reverses high-fat diet induced metabolic derangement and oxidative stress. Front Biosci (Elite Ed). 2021a;13(1):54-76. doi: 10.2741/872.
42. Jin D, Jin S, Zhou T, Sheng G, Gao P, Li G. Effects of Quercetin on Metabolic Dysfunction-Associated Steatotic Liver Disease: A Systematic Review and Meta-Analysis. Food Sci Nutr. 2025 Dec 15;13(12):e71358. doi: 10.1002/fsn3.71358.
43. Zhu M, Zhou X, Zhao J. Quercetin prevents alcohol-induced liver injury through targeting of PI3K/Akt/nuclear factor-κB and STAT3 signaling pathway. Exp Ther Med. 2017 Dec;14(6):6169-6175. doi: 10.3892/etm.2017.5329.
44. Sun Y, Ge X, Li X, He J, Wei X, Du J, Sun J, Li X, Xun Z, Liu W, Zhang H, Wang ZY, Li YC. High-fat diet promotes renal injury by inducing oxidative stress and mitochondrial dysfunction. Cell Death Dis. 2020 Oct 24;11(10):914. doi: 10.1038/s41419-020-03122-4.

45. Esquinas P, Rios R, Raya AI, Pineda C, Rodriguez M, Aguilera-Tejero E, Lopez I. Structural and ultrastructural renal lesions in rats fed high-fat and high-phosphorus diets. Clin Kidney J. 2020 Feb 18;14(3):847-854. doi: 10.1093/ckj/sfaa009.

Cite as: Onaolapo AY, Akinrinde ES, Wahab KA, Olofinnade AT, Onaolapo OJ, Histopathological and Computational Histomorphometric Evaluation of the Protective Effects of Quercetin in High-Fat High-Sugar Diet-Induced Metabolic Syndrome in Wistar Rats Acta Bioscientia **2026**:2(4);458-472. https://doi.org/10.71181/actabioscientia12610